

The revision of the manuscript provides an improvement from the earlier version. However, there remains problems w.r.t.

1 **Modelling spatial and temporal dynamics of GPP in the Sahel from** *Redundancy, sentence*
2 **earth observation based photosynthetic capacity and quantum** *structure, etc. The*
3 **efficiency** *manuscript could benefit from professional editing.*

4
5 Torben Tagesson¹, Jonas Ardö², Bernard Cappelaere³, Laurent Kergoat⁴, Abdulhakim Abdi²,
6 Stéphanie Horion¹, Rasmus Fensholt¹

7
8 ¹Department of Geosciences and Natural Resource Management, University of Copenhagen, Øster Voldgade 10, DK-
9 1350 Copenhagen, Denmark; E-Mails: torben.tagesson@ign.ku.dk, stephanie.horion@ign.ku.dk, rf@ign.ku.dk

10
11 ²Department of Physical Geography and Ecosystem Science, Lund University, Sölvegatan 12, SE- 223 62 Lund,
12 Sweden, E-Mails: jonas.ardo@nateko.lu.se, hakim.abdi@gmail.com

13
14 ³HydroSciences Montpellier, IRD, CNRS, Univ. Montpellier, Montpellier, France, E-Mail: bernard.cappelaere@um2.fr

15
16 ⁴Geoscience Environnement Toulouse, (CNRS/UPS/IRD), 14 av E Belin, 31400 Toulouse, France, E-
17 Mail: laurent.kergoat@get.obs-mip.fr

18

19 *Correspondence to:* Torben Tagesson (torben.tagesson@ign.ku.dk)

20 **Abstract.** It has been shown that vegetation growth in semi-arid regions is important ~~for the variability~~ ^{for the} of the global
21 terrestrial CO₂ sink, which indicates the strong need for improved understanding, and spatially explicit estimates of CO₂
22 uptake (gross primary production (GPP)) in semi-arid ecosystems. This study has three aims: 1) to evaluate the
23 MOD17A2H GPP (collection 6) product against eddy covariance (EC) based GPP for six sites across the Sahel; 2) to
24 characterise relationships between spatial and temporal variability in EC based photosynthetic capacity (F_{opt}) and
25 quantum efficiency (α) and earth observation (EO) based vegetation indices (normalized difference vegetation index
26 (NDVI); renormalized difference vegetation index (RDVI); enhanced vegetation index (EVI); and shortwave infrared
27 water stress index (SIWSI)); and 3) to study the applicability of EO up-scaled F_{opt} and α for GPP modelling purposes.
28 MOD17A2H GPP (collection 6) underestimated GPP strongly, most likely because maximum light use efficiency is set
29 too low for semi-arid ecosystems in the MODIS algorithm. Intra-annual dynamics in F_{opt} was closely related to SIWSI
30 being sensitive to equivalent water thickness, whereas α was closely related to RDVI affected by chlorophyll
31 abundance. Spatial and inter-annual dynamics in F_{opt} and α were closely coupled to NDVI and RDVI, respectively.
32 Modelled GPP based on F_{opt} and α up-scaled using EO based indices reproduced in situ GPP well for all except a
33 cropped site that was strongly impacted by anthropogenic land use. Up-scaled GPP for Sahel 2001-2014 was 736 ± 39 g
34 C m⁻² y⁻¹. This study indicates the strong applicability of EO as a tool for spatially explicit estimates of GPP, F_{opt} and α ;
35 incorporating EO-based F_{opt} and α in to dynamic global vegetation models could improve global estimates of vegetation
36 production, ecosystem processes and biogeochemical and hydrological cycles.

37

38 **Keywords:** Remote sensing, Gross Primary Productivity, MOD17A2H, light use efficiency, photosynthetic capacity,
39 quantum efficiency

40 **1 Introduction**

41 Vegetation growth in semi-arid regions is an important sink for fossil fuel emissions. Mean carbon dioxide (CO₂)
42 uptake by terrestrial ecosystems is dominated by highly productive lands, mainly tropical forests, whereas semi-arid
43 regions are the main biome driving its inter-annual variability (Ahlström et al., 2015; Poulter et al., 2014). Semi-arid
44 regions even contribute to 60% of the long term trend in the global terrestrial C sink (Ahlström et al., 2015). It is thus
45 important to understand long-term variability of vegetation growth in semi-arid areas and their response to
46 environmental conditions to better quantify and forecast effects of climate change.

47 Sahel is a semi-arid transition zone between the dry Sahara desert in the North and the humid Sudanian savanna in the
48 South. The region has experienced numerous severe droughts during the last decades that resulted in region-wide
49 famines in 1972-1973 and 1984-1985 and localized food shortages across the region in 1990, 2002, 2004, 2011 and
50 2012 (Abdi et al., 2014; United Nations, 2013). Vegetation production is thereby an important ecosystem service for
51 livelihood in Sahel, but it is under threat. The region experiences a strong population growth, increasing the demand on
52 ecosystem services due to cropland expansion, increased pasture stocking rates and fuelwood extraction (Abdi et al.,
53 2014).

54 At the same time as we have reports of declining vegetation production, we have contradicting reports of greening of
55 the Sahel based on earth observation (EO) data (Dardel et al., 2014; Fensholt et al., 2013). The greening of Sahel has
56 mainly been attributed to alleviated drought stress conditions due to increased precipitation since the mid-1990s
57 (Hickler et al., 2005). Climate is thus another important factor regulating vegetation production. Semi-arid regions, such
58 as Sahel, are particularly vulnerable to climate fluctuations due to their dependency ~~to~~ ^{on} moisture ~~conditions~~ ✓ ✗

59 Estimation of gross primary production (GPP), i.e. uptake of atmospheric CO₂ by vegetation, is still a major challenge
60 within remote sensing of ecosystem services. Gross primary production is a main driver of ecosystem services such as
61 climate regulation, carbon (C) sequestration, C storage, food production, or livestock grassland production. Within EO,
62 spatial quantification of GPP generally involves light use efficiency (LUE), defined as the conversion efficiency of
63 absorbed solar light into CO₂ uptake (Monteith, 1972, 1977). It has been shown that LUE varies in space and time due
64 to factors such as plant functional type, drought and temperature, nutrient levels and physiological limitations of
65 photosynthesis (Garbulsky et al., 2010; Paruelo et al., 2004; Kergoat et al., 2008). The LUE concept has been applied
66 using various methods, either by using a biome-specific LUE constant (Ruijmy et al., 1994), or by modifying a
67 maximum LUE using meteorological variables (Running et al., 2004).

68 An example of an LUE based model is the standard GPP product from the Moderate Resolution Imaging
69 Spectroradiometer (MODIS) sensor (MOD17A2). Within the model, absorbed photosynthetically active radiation
70 (PAR) is estimated as a product of the fraction of PAR absorbed by green vegetation (FPAR from MOD15A2)
71 multiplied with daily PAR from the meteorological data of the Global Modeling and Assimilation Office (GMAO). A
72 set of maximum LUE parameters specified for each biome are extracted from a Biome Properties Look-Up Table
73 (BPLUT). Then maximum LUE is modified depending on air temperature (T_{air}) and vapor pressure deficit (VPD)
74 (Running et al., 2004). Sjöström et al. (2013) evaluated the MOD17A2 product (collection 5.1) for Africa, and showed

— X

75 that it underestimated GPP for semi-arid savannas in Sahel. Explanations for this underestimation were that the assigned
76 maximum LUE from BPLUT was set too low and uncertainties in the FPAR (MOD15A2) product. Recently, a new
77 collection of MOD17A2 at 500 m spatial resolution was released (MOD17A2H; collection 6) with an updated BPLUT,
78 updated GMAO meteorological data, improved quality control and gap filling of the FPAR data from MOD15A2
79 (Running and Zhao, 2015).

80 It has been shown that the LUE method does not perform well in arid conditions and at agricultural sites (Turner et
81 al., 2005). Additionally, the linearity assumed by the LUE model is usually not found as the response of GPP to
82 incoming light follows more of an asymptotic curve (Cannell and Thornley, 1998). Investigating other methods for
83 remotely determining GPP is thus of great importance, especially for semi-arid environments. Therefore, instead of
84 LUE we focus on the light response function of GPP at canopy scale, and spatial and temporal variation of its two main
85 parameters: maximum GPP under light saturation (canopy-scale photosynthetic capacity; F_{opt}), and the initial slope of
86 the light response function (canopy-scale quantum efficiency; α) (Falge et al., 2001; Tagesson et al., 2015a).
87 Photosynthetic capacity is a measure of the maximum rate at which the canopy can fix CO₂ during photosynthesis
88 ($\mu\text{mol CO}_2 \text{ m}^{-2} \text{ s}^{-1}$) whereas α is the amount of CO₂ fixed per incoming PAR ($\mu\text{mol CO}_2 \mu\text{mol PAR}^{-1}$). Just to clarify the
89 difference in LUE and α in this study; LUE ($\mu\text{mol CO}_2 \mu\text{mol APAR}^{-1}$) is the slope of a linear fit between CO₂ uptake
90 and absorbed PAR, whereas α ($\mu\text{mol CO}_2 \mu\text{mol PAR}^{-1}$) is the initial slope of an asymptotic curve against incoming
91 PAR.

92 It has been proven that F_{opt} and α are closely related to chlorophyll abundance due to their coupling with the electron
93 transport rate (Ide et al., 2010). Additionally, in semi-arid ecosystems water availability is generally considered to be
94 the main limiting factor affecting intra-annual dynamics of vegetation growth (Fensholt et al., 2013; Hickler et al.,
95 2005; Tagesson et al., 2015b). Several remote sensing studies have established relationships between remotely sensed
96 vegetation indices and ecosystem properties such as chlorophyll abundance and equivalent water thickness (Yoder and
97 Pettigrew-Crosby, 1995; Fensholt and Sandholt, 2003). In this study we will analyse if EO vegetation indices can be
98 used for up-scaling F_{opt} and α and investigate if this could offer a promising way to map GPP in semi-arid areas. This
99 potential will be analysed by the use of detailed ground observations from six eddy covariance (EC) flux tower sites
100 across Sahel.

101 The three aims of this study are:

- 102 1) To investigate if the recently released MOD17A2H GPP (collection 6) product is better at capturing GPP for
103 Sahel than collection 5.1. We hypothesise that MOD17A2H GPP (collection 6) product will estimate GPP well
104 for the six Sahelian EC sites, because of major changes done in comparison to collection 5.1 (Running and
105 Zhao, 2015).
- 106 2) To characterize the relationships between spatial and temporal variability in F_{opt} and α and remotely sensed
107 vegetation indices. We hypothesise that EO vegetation indices that are closely related to chlorophyll
108 abundance will be most strongly coupled with spatial and inter-annual dynamics in F_{opt} and α , whereas
109 vegetation indices closely related to equivalent water thickness will be most strongly coupled with intra-annual
110 dynamics in F_{opt} and α across Sahel.
- 111 3) To evaluate the applicability of a GPP model based on the light response function using EO vegetation indices
112 and incoming PAR as input data.

113

114 **2 Materials and Methods**

115 **2.1 Site description**

116 The Sahel stretches from the Atlantic Ocean in the west to the Red Sea in the east. The northern border towards Sahara
117 and the southern border towards the humid Sudanian Savanna are defined by the 150 and 700 mm isohyets, respectively
118 (Fig. 1) (Prince et al., 1995). Tree and shrub canopy cover is now generally low (< 5%) and dominated by species of
119 *Balanites*, *Acacia*, *Boscia* and *Combretaceae* (Rietkerk et al., 1996). Annual grasses such as *Schoenoplectus gracilis*,
120 *Dactyloctenium aegypticum*, *Aristida mutabilis*, and *Cenchrus biflorus* dominate the herbaceous layer, but perennial
121 grasses such as *Andropogon gayanus*, *Cymbopogon schoenanthus* can also be found (Rietkerk et al., 1996; de Ridder et
122 al., 1982). From the FLUXNET database (Balocchi et al., 2001) we selected the six available measurement sites with
123 EC based CO₂ flux data from Sahel (Table 1; Fig. 1). The sites represent a variety of ecosystems present in the region,
124 from dry fallow bush savanna to seasonally inundated acacia forest. For a full description of the measurement sites, we
125 refer to Tagesson et al. (2016a) and references in Table 1.

126 <Table 1>

127 <Figure 1>

128

129 **2.2 Data collection**

130 **2.2.1 Eddy covariance and hydrometeorological in situ data**

131 Eddy covariance and hydrometeorological data originating from the years between 2005 and 2013 were collected from
132 the principal investigators of the measurement sites (Tagesson et al., 2016a). The EC sensor set-up consisted of open-
133 path CO₂/H₂O infrared gas analysers and 3-axis sonic anemometers. Data were collected at 20 Hz rate and statistics
134 were calculated for 30-min periods. For a full description of sensor set up and post processing of EC data, see
135 references in Table 1. Final fluxes were filtered according to quality flags provided by FLUXNET and outliers were
136 filtered according to Papale et al. (2006). We extracted the original net ecosystem exchange (NEE) data without any
137 gap-filling or partitioning of NEE to GPP and ecosystem respiration. The collected hydrometeorological data were: air
138 temperature (T_{air}; °C), rainfall (P; mm), relative air humidity (Rh; %), soil moisture at 0.1 m depth (SWC; % volumetric
139 water content), incoming global radiation (R_g; W m⁻²), incoming photosynthetically active radiation (PAR; μmol m⁻² s⁻¹),
140 VPD (hPa), peak dry weight biomass (g dry weight m⁻²), C3/C4 species ratio, and soil conditions (nitrogen and C
141 concentration; %). For a full description of collected data and sensor set-up, see Tagesson et al. (2016a).

142

143 **2.2.2 Earth Observation data and gridded ancillary data**

144 Composite products from MODIS/Terra covering Sahel were acquired at Reverb ECHO (NASA, 2016). Collected
145 products were GPP (MOD17A2H; collection 6), nadir bidirectional reflectance distribution function adjusted
146 reflectance (NBAR) (8-day composites; MCD43A4; collection 5.1) at 500¹⁰500 m² spatial resolution, the normalized
147 difference vegetation index (NDVI) and the enhanced vegetation index (EVI) (16-day composites; MOD13Q1;
148 collection 6) at 250¹⁰250 m² spatial resolution. The NBAR product was preferred over the reflectance product
149 (MOD09A1), in order to avoid variability caused by varying sun and sensor viewing geometry (Huber et al., 2014;
150 Tagesson et al., 2015c). We extracted the median of 3x3 pixels centred at the location of each EC tower. Time series of
151 EO products were filtered according to MODIS quality control data; MOD17A2H is a gap-filled and filtered product,

152 QC data from MCD43A2 were used for filtering of MCD43A4; and bit 2-5 (highest –decreasing quality) was used for
153 MOD13Q1. Finally, data were gap-filled to daily values using linear interpolation.

154 We downloaded ERA Interim reanalysis PAR at the ground surface (W m^{-2}) with a spatial resolution of $0.25^\circ \times 0.25^\circ$
155 accumulated for each 3-hour period 2000-2015 from the European Centre for Medium-Range Weather Forecasts
156 (ECMWF) (Dee et al., 2011; ECMWF, 2016a).

157

158 **2.3 Data handling**

159 **2.3.1 Intra-annual dynamics in photosynthetic capacity and quantum efficiency**

160 To estimate daily values of EC based F_{opt} and α , the asymptotic Mitscherlich light-response function was fitted between
161 daytime NEE and incoming PAR using a 7-day moving window with a 1-day time step:

$$162 \text{NEE} = -(F_{\text{opt}}) \times (1 - e^{\left(\frac{-\alpha \text{PAR}}{F_{\text{opt}}}\right)}) + R_d \quad (1)$$

163 where F_{opt} is CO_2 uptake at light saturation (photosynthetic capacity; $\mu\text{mol CO}_2 \text{ m}^{-2} \text{ s}^{-1}$), R_d is dark respiration
164 ($\mu\text{mol CO}_2 \text{ m}^{-2} \text{ s}^{-1}$), and α is the initial slope of the light response curve (quantum efficiency; $\mu\text{mol CO}_2 \mu\text{mol PAR}^{-1}$)
165 (Falge et al., 2001). By subtracting R_d from Eq. 1, the function was forced through zero and GPP was thereby estimated.
166 To assure high quality of fitted parameters, parameters were excluded from the analysis when fitting was insignificant
167 ($p\text{-value} > 0.05$), and when they were out of range (F_{opt} and $\alpha >$ peak value of the rainy season times 1.2). Additionally,
168 outliers were filtered following the method by Papale et al. (2006) using a 30-day moving window with a 1-day time
169 step.

170

171 **2.3.2 Vegetation indices**

172 The maximum absorption in red wavelengths generally occurs at 682 nm as this is the peak absorption for chlorophyll a
173 and b (Thenkabail et al., 2000), which makes vegetation indices that include the red band sensitive to chlorophyll
174 abundance. By far the most common vegetation index is NDVI (Rouse et al., 1974):

$$175 \text{NDVI} = \frac{(\rho_{\text{NIR}} - \rho_{\text{red}})}{(\rho_{\text{NIR}} + \rho_{\text{red}})} \quad (2)$$

176 where ρ_{NIR} is the reflectance factor in near infrared (NIR) band (band 2) and ρ_{red} is the reflectance factor in the red band
177 (band 1). Near infrared radiance is reflected by leaf cells since absorption of these wavelengths would result in
178 overheating of the plant whereas red radiance is absorbed by chlorophyll and its accessory pigments (Gates et al., 1965).
179 Normalization is done to reduce effects of atmospheric errors, solar zenith angles, and sensor viewing geometry, as well
180 as increasing the vegetation signal (Qi et al., 1994; Inoue et al., 2008).

181 A well-known deficiency of NDVI is problems of index saturation at high biomass because absorption of red light at
182 ~ 670 nm peaks at higher biomass loads whereas NIR reflectance continues to increase due to multiple scattering effects
183 (Mutanga and Skidmore, 2004; Jin and Eklundh, 2014). By reducing atmospheric and soil background influences, EVI
184 is designed to increase the signal from the vegetation and maintain sensitivity in high biomass regions (Huete et al.,
185 2002).

$$186 \text{EVI} = G \frac{(\rho_{\text{NIR}} - \rho_{\text{red}})}{(\rho_{\text{NIR}} + C_1 \rho_{\text{red}} - C_2 \rho_{\text{blue}} + L)} \quad (3)$$

187 where ρ_{blue} is the reflectance factor in the blue band (band 3). The coefficients $C_1=6$ and $C_2=7.5$ correct for atmospheric
188 influences, while $L=1$ adjust for the canopy background. The factor $G=2.5$ is a gain factor.

189 Another attempt to overcome problems of NDVI saturation was proposed by Roujean and Breon (1995) who
190 suggested the renormalized difference vegetation index (RDVI) that combines advantages of DVI (NIR-red) and NDVI
191 for low and high vegetation cover, respectively:

$$192 \quad RDVI = \frac{(\rho_{NIR} - \rho_{red})}{\sqrt{(\rho_{NIR} + \rho_{red})}} \quad (4)$$

193 As a non-linear index, RDVI is not only less sensitive to variations in geometrical and optical properties of unknown
194 foliage but also less affected by solar and viewing geometry (Broge and Leblanc, 2001). RDVI was calculated based on
195 NBAR bands 1 and 2.

196 The NIR and SWIR bands are affected by the same ground properties, except that SWIR bands are also strongly
197 sensitive to equivalent water thickness. Fensholt and Sandholt (2003) proposed a vegetation index, the shortwave
198 infrared water stress index (SIWSI), using NIR and SWIR bands to estimate drought stress for vegetation in semi-arid
199 environments:

$$200 \quad SIWSI_{12} = \frac{(\rho_{NIR} - \rho_{SWIR12})}{\rho_{NIR} + \rho_{SWIR12}} \quad (5)$$

$$201 \quad SIWSI_{16} = \frac{(\rho_{NIR} - \rho_{SWIR16})}{\rho_{NIR} + \rho_{SWIR16}} \quad (6)$$

202 where ρ_{swir12} is NBAR band 5 (1230-1250 nm) and ρ_{swir16} is NBAR band 6 (1628-1652 nm). As the vegetation water
203 content increases, reflectance in SWIR decreases indicating that low and high SIWSI values point to sufficient water
204 conditions and drought stress, respectively.

205 206 2.3.3 Incoming PAR across Sahel

207 A modified version of the ERA Interim reanalysis PAR was used in the current study as an error in the code producing
208 these PAR estimates was identified by the data distributor causing PAR values to be too low (ECMWF, 2016b).
209 Accordingly, incoming PAR at the ground surface from ERA Interim was systematically underestimated even though it
210 followed the pattern of PAR measured at the six Sahelian EC sites (Fig. S1 in supplementary material). In order to
211 correct for this error, we fitted and applied an ordinary least square linear regression between in situ PAR and ERA
212 Interim PAR (Fig. S1). The produced PAR from this relationship is at the same level as in situ PAR and should be at a
213 correct level even though the original ERA Interim PAR is actually produced from the red and near infrared part of the
214 spectrum.

215 216 2.4 Data analysis

217 2.4.1 Coupling temporal and spatial dynamics in photosynthetic capacity and quantum efficiency with 218 explanatory variables

219 The coupling between intra-annual dynamics in F_{opt} and α and the vegetation indices for the different measurement sites
220 were studied using Pearson correlation analysis. As part of the correlation analysis, we used bootstrap simulations with
221 200 iterations from which mean and standard deviation of the correlation coefficients were calculated (Richter et al.,

The vegetation index
(4)

Never
start a
sentence
with an
acronym,
#, or symbol
Change as
was intended!

the estimates were
generally too low.

↑ also addressed on
p. 1258-261.
eliminate
redundancy!

222 2012). Relationships between intra-annual dynamics in F_{opt} and α and the vegetation indices for all sites combined were
 223 also analysed. In the analysis for all sites, data were normalised in order to avoid influence of spatial and inter-annual
 224 variability. Time series of ratios of F_{opt} and α (F_{opt_frac} and α_{frac}) against the annual peak values (F_{opt_peak} and α_{peak} ; see
 225 below for calculation of annual peak values) were estimated for all sites:

$$226 \quad F_{opt_frac} = \frac{F_{opt}}{F_{opt_peak}} \quad (7)$$

$$227 \quad \alpha_{frac} = \frac{\alpha}{\alpha_{peak}} \quad (8)$$

228 The same standardisation procedure was used for all vegetation indices (VI_{frac}):

$$229 \quad VI_{frac} = \frac{VI}{VI_{peak}} \quad (9)$$

230 where VI_{peak} is the annual peak values of the vegetation indices (14 days running mean with highest annual value). The
 231 coupling between α_{frac} and F_{opt_frac} and the different VI_{frac} were examined using Pearson correlation analysis for all sites.

232 Regression trees were used to fill gaps in the daily estimates of F_{opt} and α . One hundred tree sizes were chosen based
 233 on 100 cross validation runs, and these trees were then used for estimating F_{opt} and α following the method in De'ath
 234 and Fabricius (2000). We used SWC, VPD, T_{air} , PAR, and the vegetation index with strongest correlation with intra-
 235 annual dynamics as explanatory variables in the analysis. In the analysis for all sites, the same standardisation procedure
 236 as done for F_{opt} , α , and the vegetation indices was done for the hydrometeorological variables. The 100 F_{opt} and α output
 237 subsets from the regression trees were averaged and used for filling gaps in the times series of F_{opt} and α . From these
 238 time-series we estimated annual peak values of F_{opt} and α (F_{opt_peak} and α_{peak}) as the 14-day running mean with highest
 239 annual value. To investigate spatial and inter-annual variability in F_{opt} and α across the measurement sites of the Sahel,
 240 F_{opt_peak} and α_{peak} were correlated with the annual sum of P, yearly means of T_{air} , SWC, RH, VPD, R_g , annual peak
 241 values of biomass, soil nitrogen and C concentrations, C3/C4 ratio, and VI_{peak} using Pearson linear correlations.

242

243 **2.4.2 Parameterisation and evaluation of the GPP model and evaluation of the MODIS GPP**

244 Based on Eq. 1 and outcome of the statistical analysis previously described under subsection 2.4.1 (for results see
 245 subsect. 3.2), a model for estimating GPP across Sahel was created:

$$246 \quad GPP = -F_{opt} \times (1 - e^{\left(\frac{-\alpha \times PAR}{F_{opt}} \right)}) \quad (10)$$

247 Firstly, F_{opt_peak} and α_{peak} were estimated spatially and inter-annually using linear regression functions fitted against the
 248 vegetation indices with strongest relationships to spatial and inter-annual variability in F_{opt_peak} and α_{peak} for all sites.
 249 Secondly, exponential regression functions were established for F_{opt_frac} and α_{frac} with the vegetation index with the
 250 strongest relationships to intra-annual variability of F_{opt_frac} and α_{frac} for all sites. By combining these relationships, F_{opt}
 251 and α can be calculated for any day of year and for any point in space across Sahel:

$$252 \quad F_{opt} = F_{opt_peak} \times F_{opt_frac} = \left(k_{F_{opt}} \times NDVI_{peak} + m_{F_{opt}} \right) \left(n_{F_{opt}} \times e^{(l_{F_{opt}} \times RDVI_{frac})} \right) \quad (11)$$

$$253 \quad \alpha = \alpha_{peak} \times \alpha_{frac} = \left(k_{\alpha} \times RDVI_{peak} + m_{\alpha} \right) \left(n_{\alpha} \times e^{(l_{\alpha} \times RDVI_{frac})} \right) \quad (12)$$

redundant
see p.6
J. 219-
220.

254 where $k_{F_{opt}}$ and k_a are slopes and $m_{F_{opt}}$ and m_a are intercepts of the linear regressions giving F_{opt_peak} and a_{peak} ,
 255 respectively; $l_{F_{opt}}$ and l_a are coefficients and $n_{F_{opt}}$ and n_a are intercepts of the exponential regressions giving F_{opt_frac} and
 256 a_{frac} , respectively. Equation 11 and 12 were inserted into Eq. 10 and GPP were thereby estimated as:

$$257 GPP = -\left(F_{opt_peak} \times F_{opt_frac}\right) \times \left(1 - e^{\left(\frac{-(a_{peak} \times a_{frac}) \times PAR}{F_{opt_peak} \times F_{opt_frac}}\right)}\right) = -\left(\left(k_{F_{opt}} \times NDVI_{peak} + m_{F_{opt}}\right) \left(n_{F_{opt}} \times e^{\left(l_{F_{opt}} \times RDVI_{frac}\right)}\right)\right) \\ \times \left(1 - e^{\left(\frac{-(k_a \times RDVI_{peak} + m_a) \left(n_a \times e^{\left(l_a \times RDVI_{frac}\right)}\right) \times PAR}{\left(k_{F_{opt}} \times NDVI_{peak} + m_{F_{opt}}\right) \left(l_{F_{opt}} \times RDVI_{frac} + n_{F_{opt}}\right)}\right)}\right) \quad (13)$$

redundant

258 A bootstrap simulation methodology with 200 iterations was used when fitting the least-square regression functions
 259 for parameterisation of the GPP model (Richter et al., 2012). For each of the iterations, some of the EC sites were
 260 included and some were left-out. The bootstrap simulations generated 200 sets of $k_{F_{opt}}$, k_a , $m_{F_{opt}}$, m_a , $l_{F_{opt}}$, l_a , $n_{F_{opt}}$, n_a ,
 261 and coefficient of determination (R^2), from which the medians and the standard deviations were estimated. Possible
 262 errors (e.g. random sampling errors, aerosols, electrical sensor noise, filtering and gap-filling errors, clouds, and satellite
 263 sensor degradation) can be present in both the predictor and the response variables. Hence, we selected reduced major
 264 axis regressions to account for errors in both predictor and response variables when fitting the regression functions. The
 265 regression models were validated against the left-out sites within the bootstrap simulation methodology by calculating
 266 the root-mean-square-error (RMSE), and by fitting an ordinary least squares linear regression between modelled and
 267 independent variables.

268 Similarly, the MODIS GPP product (MOD17A2H, collection 6) was evaluated against independent GPP from the EC
 269 sites by calculating RMSE, and by fitting an ordinary least squares linear regression.

270

271 3 Results

272 3.1 Evaluation of the MODIS GPP product

273 There was a strong linear relationship between the MODIS GPP product (MOD17A2H; collection 6) and independent
 274 GPP (slope=0.17; intercept=0.11 g C m⁻² d⁻¹; R^2 =0.69; n=598). However, MOD17A2H strongly underestimated
 275 independent GPP (Fig. 2) resulting in high RMSE (2.69 g C m⁻² d⁻¹). It can be seen that some points for the Kelma site
 276 were quite low for MOD17A2H, whereas they were relatively high for the independent GPP (Fig. 2). Kelma is an
 277 inundated Acacia forest located in a clay soil depression. These differentiated values were found in the beginning of the
 278 dry season, when the depression was still inundated, whereas the larger area was turning dry.

279 <Figure 2>

280

281 3.2 Intra-annual dynamics in photosynthetic capacity and quantum efficiency

282 Intra-annual dynamics in F_{opt} and a differed in amplitude, but were otherwise similar across the measurement sites in
 283 Sahel (Fig. 3). There was no green ground vegetation during the dry season, and the low photosynthetic activity was
 284 due to few evergreen trees. This resulted in low values for both F_{opt} and a during the dry season. The vegetation
 285 responded strongly to rainfall, and both F_{opt} and a increased during the early phase of the rainy season. Generally, F_{opt}
 286 peaked slightly earlier than a (average± 1 standard deviation: 7±10 days) (Fig. 3).

287 <Figure 3>

reasonably well

288 All vegetation indices described ~~well~~ intra-annual dynamics in F_{opt} for all sites (Table 2). SIWSI₁₂ had the highest
289 correlation for all sites except Wankama Millet, where it was RDVI. When all sites were combined, all indices
290 described well seasonality in F_{opt} , but RDVI had the strongest correlation (Table 2). — X

291 Intra-annual dynamics in α were also closely coupled to intra-annual dynamics in the vegetation indices for all sites
292 (Table 2). For α , RDVI was the strongest index describing intra-annual dynamics, except for Wankama Fallow where it
293 was EVI. When all sites were combined all indices described well intra-annual dynamics in α , but RDVI was still the
294 index with strongest relationship (Table 2).

295 <Table 2>

296 The regression trees used for gap-filling explained ~~well~~ the intra-annual dynamics in F_{opt} and α for all sites (Table 3;
297 Fig. S2 in Supplementary material). The regression trees explained intra-annual dynamics in F_{opt} better than in α , and
298 multi-year sites were better predicted than single year sites (Fig. S2). The main explanatory variables coupled to intra-
299 annual dynamics in F_{opt} for all sites across Sahel were in the order of RDVI, SWC, VPD, T_{air} , and PAR; and for α they
300 were RDVI, SWC, VPD and T_{air} (Table 3). The strong relationship to SWC and VPD indicates drought stress during
301 periods of low rainfall. For all sites across Sahel, incorporating hydrometeorological variables increased the ability to
302 determine intra-annual dynamics in F_{opt} and α compared to the ordinary least squares linear regressions against
303 vegetation indices (Table 2, data given as r ; Table 3; Fig. 3 and Fig. S2). For all sites, incorporation of these variables
304 increased R^2 from 0.81 to 0.87 and from 0.74 to 0.84, for F_{opt} and α respectively. — X

305 <Table 3>

306

307 3.3 Spatial and inter-annual dynamics in photosynthetic capacity and quantum efficiency

308 Large spatial and inter-annual variability in F_{opt_peak} and α_{peak} were found across the six measurement sites in Sahel;
309 F_{opt_peak} ranged between 10.1 $\mu\text{mol CO}_2 \text{ m}^{-2} \text{ s}^{-1}$ (Wankama Millet 2005) and 50.0 $\mu\text{mol CO}_2 \text{ m}^{-2} \text{ s}^{-1}$ (Dahra 2010), and
310 α_{peak} ranged between 0.020 $\mu\text{mol CO}_2 \mu\text{mol PAR}^{-1}$ (Demoekeya 2007) and 0.064 $\mu\text{mol CO}_2 \mu\text{mol PAR}^{-1}$ (Dahra 2010)
311 (Table 4). The average two week running mean peak values of F_{opt} and α for all sites were 26.4 $\mu\text{mol CO}_2 \text{ m}^{-2} \text{ s}^{-1}$ and
312 0.040 $\mu\text{mol CO}_2 \mu\text{mol PAR}^{-1}$, respectively. All vegetation indices determined ~~well~~ spatial and inter-annual dynamics in
313 F_{opt_peak} and α_{peak} (Table 5). $NDVI_{peak}$ was most closely coupled with F_{opt_peak} , whereas $RDVI_{peak}$ was ~~closest~~ coupled with
314 α_{peak} (Fig. 4). F_{opt_peak} also correlated well with peak dry weight biomass, C content in the soil, and RH, whereas α_{peak}
315 also correlated well with peak dry weight biomass, and C content in the soil (Table 5). well X

316 <Table 4>

317 <Table 5>

318 <Figure 4>

319

320 3.4 Spatially extrapolated photosynthetic capacity, quantum efficiency, and gross primary production across 321 Sahel and evaluation of the GPP model

322 The spatially extrapolated F_{opt} , α and GPP averaged over Sahel for 2001-2014 were $22.5 \pm 1.7 \mu\text{mol CO}_2 \text{ m}^{-2} \text{ s}^{-1}$,
323 $0.030 \pm 0.002 \mu\text{mol CO}_2 \mu\text{mol PAR}^{-1}$, and $736 \pm 39 \text{ g C m}^{-2} \text{ y}^{-1}$, respectively. At regional scale it can be seen that F_{opt} , α ,
324 and GPP decreased substantially with latitude (Fig. 5). Highest values were found in south-eastern Senegal, western
325 Mali, in parts of southern Sudan and on the border between Sudan and South Sudan. Lowest values were found along
326 the northernmost parts of Sahel on the border to Sahara in Mauritania, in northern Mali, and in northern Niger. more closely

327 Modelled GPP was similar to independent GPP on average, and there was a strong linear relationship between
328 modelled GPP and independent GPP for all sites (Fig. 6; Table 6). However, when separating the evaluation between
329 measurement sites, it can be seen that the model reproduced some sites better than others (Fig. 7; Table 6). Wankama
330 Millet was generally overestimated  whereas the model worked well on average for Demokeya but underestimated high
331 values (Fig. 7; Table 6). Variability of independent GPP at the other sites was well reproduced by the model (Fig. 7;
332 Table 6). The final parameters of the GPP model (Eq. 13) are given in Table 7. 

333 <Figure 5>

334 <Figure 6>

335 <Figure 7>

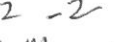
336 < Table 6>

337 < Table 7>

338

339 **4 Discussions**

340 Our hypothesis that vegetation indices closely related to equivalent water thickness (SIWSI) would be most strongly
341 coupled with intra-annual dynamics in F_{opt} and α was not rejected for F_{opt} , since this was the case for all sites except for
342 Wankama Millet (Table 2). However, our hypothesis was rejected for α , since it was more closely related to vegetation
343 indices related to chlorophyll abundance (RDVI and EVI). In Sahel, soil moisture conditions in the early rainy season
344 are important for vegetation growth and during this phase vegetation is especially vulnerable to drought conditions
345 (Rockström and de Rouw, 1997; Tagesson et al., 2016a; Mbow et al., 2013). Photosynthetic capacity (F_{opt}) peaked
346 earlier in the rainy season than α did (Fig. 3), thereby explaining the close relationship of F_{opt} to SIWSI. Leaf area index
347 increased over the growing season and leaf area index  was closely coupled with vegetation indices related to chlorophyll
348 abundance (Tagesson et al., 2009). The increase in leaf area index increased canopy level quantum efficiency (α), which
349 thereby explains the closer relationship of α to RDVI.

350 Our hypothesis that vegetation indices closely related to chlorophyll abundance would be most strongly coupled with
351 spatial and inter-annual dynamics in F_{opt} and α was not rejected for either F_{opt} or α ; NDVI, EVI, and RDVI ~~all had close~~
352 correlation with spatial and inter-annual dynamics in F_{opt} and α (Table 5). However, it was surprising that $NDVI_{peak}$ had
353 the strongest correlation with spatial and inter-annual variability for F_{opt} (Table 5). Both EVI and RDVI should be less
354 sensitive to saturation effects than NDVI (Huete et al., 2002; Roujean and Breon, 1995), and based on this it can be
355 assumed that peak values of these indices should have stronger relationships to peak values of F_{opt} and α . However,
356 vegetation indices with a high sensitivity to changes in green biomass at high biomass loads, gets less sensitive to green
357 biomass changes at low biomass loads (Huete et al., 2002). Peak leaf area index for ecosystems across Sahel is
358 generally ~2, or less, whereas the saturation issue of NDVI generally starts at a leaf area index of about 2-5   
359 (Haboudane et al., 2004).

360 The F_{opt_peak} estimates from Agoufou, Demokeya, and the Wankama sites were similar whereas Dahra and Kelma
361 values were high in relation to previously reported canopy-scale F_{opt_peak} from Sahel (~8 to -23 $\mu\text{mol m}^{-2} \text{ sec}^{-1}$) (Hanafi
362 et al., 1998; Merbold et al., 2009; Moncrieff et al., 1997; Boulain et al., 2009; Levy et al., 1997; Monteny et al., 1997).
363 These previous studies reported much lower F_{opt} at canopy scale than at leaf scale (e.g. Levy et al. (1997): 10 vs. 44 μmol
364 $\text{m}^{-2} \text{ sec}^{-1}$; Boulain et al. (2009): 8 vs. 50 $\mu\text{mol m}^{-2} \text{ sec}^{-1}$). Leaf area index at Dahra and Kelma peaked at 2.1 and 2.7,
365 respectively (Timouk et al., 2009; Tagesson et al., 2015a), and it was substantially higher than at the above-mentioned

For this difference

366 sites. A possible explanation to high F_{opt} estimates at Dahra and Kelma could thereby be the higher leaf area index.
367 Tagesson et al. (2016b) performed a quality check of the EC data due to the high net CO₂ exchange measured at the
368 Dahra field site and explained the high values by a combination of moderately dense herbaceous C4 ground vegetation,
369 high soil nutrient availability, and a grazing pressure resulting in compensatory growth and fertilization effects. Another
370 possible explanation could be that the West African Monsoon bring a humid layer of surface air from the Atlantic,
371 possibly increasing vegetation production for the most western part of Sahel (Tagesson et al., 2016a).

372 Our model substantially overestimated GPP for Wankama Millet (Fig. 7f). Being a crop field, this site differed from
373 the other ~~studied~~ sites by its species composition, ecosystem structure, as well as land and vegetation management.
374 Crop fields in southwestern Niger are generally characterized by a rather low production resulting from decreased
375 fertility and soil loss caused by intensive land use (Cappelaere et al., 2009). These specifics of the Wankama Millet site
376 may cause the model parameterised with observations from the other study sites without this strong anthropogenic
377 influence to overestimate GPP at this site. Similar results were found by Boulain et al. (2009) when applying an up-
378 scaling model using leaf area index for Wankama Millet and Wankama Fallow. It worked well for Wankama fallow
379 whereas it was less conclusive for Wankama Millet. The main explanation was low leaf area index in millet fields
380 because of a low density of millet stands due to agricultural practice. There is extensive savanna clearing for food
381 production in Sahel (Leblanc et al., 2008; Boulain et al., 2009; Cappelaere et al., 2009). To further understand impacts
382 of this land cover change on vegetation production and land-atmosphere exchange processes, it is of urgent need for
383 more study sites covering cropped areas in this region.

384 In Demokeya, GPP was slightly underestimated for the year 2008 (Fig. 7c) because modelled F_{opt} was much lower
385 than the actual measured value in 2008 (the thick black line in Fig. 4). An improvement of the model could be to
386 incorporate some parameters that constrain or enhance F_{opt} depending on environmental stress. Indeed, the regression
387 tree analysis indicated that incorporating hydrometeorological variables increased the ability to predict both F_{opt} and α .
388 On the other hand, for spatial upscaling purposes, it has been shown that including modelled hydrometeorological
389 constraints on LUE decreases the ability to predict vegetation production due to the incorporated uncertainty in these
390 modelled variables (Fensholt et al., 2006; Ma et al., 2014). For spatial upscaling to regional scales it is therefore better
391 to simply use relationships to EO data. This is particularly the case for Sahel, one of the ~~largest~~ dryland areas in the
392 world that includes only a few sites of hydrometeorological observations.

393 The pattern seen in the spatially explicit GPP budgets (Fig. 5c) may be influenced by a range of biophysical and
394 anthropogenic factors. The clear North-South gradient is expected given the strong North-South rainfall gradient in
395 Sahel. The West African Monsoon mentioned above could also be an explanation ~~to~~ high GPP values in the western
396 part of Sahel, where values were relatively high in relation to GPP at similar latitudes in the central and eastern Sahel
397 (Fig. 5c). The areas with highest GPP are sparsely populated woodlands or shrubby savanna with a relatively dense tree
398 cover (Brandt et al., 2016). However, the ~~produced~~ maps should be used with caution as they are based on up-scaling of
399 the only six available EC sites that exist in the region; especially given the issues related to the cropped fields discussed

400 ~~above~~ Still, the average GPP budget for the entire Sahel 2001-2014 was close to an average annual GPP budget as
401 estimated for these six sites ($692 \pm 89 \text{ g C m}^{-2} \text{ y}^{-1}$) (Tagesson et al., 2016a). The range of GPP budgets in Fig. 5c is also
402 similar to previous annual GPP budgets reported from other savanna areas across the world (Veenendaal et al., 2004;
403 Chen et al., 2003; Kanniah et al., 2010; Chen et al., 2016).

404 Although MOD17A2 GPP has previously been shown to relatively well capture GPP in several different ecosystems
405 (Turner et al., 2006; Turner et al., 2005; Heinsch et al., 2006; Sims et al., 2006; Kanniah et al., 2009), it has been shown
406 to be underestimated for others (Coops et al., 2007; Gebremichael and Barros, 2006; Sjöström et al., 2013). GPP of
407 Sahelian drylands have not been well captured by MOD17A2 (Sjöström et al., 2013; Fensholt et al., 2006), and as we
408 have shown, this underestimation persists in the latest MOD17A2H GPP (collection 6) product (Fig. 2). The main
409 reason for this pronounced underestimation is that maximum LUE is set to 0.84 g C MJ^{-1} (open shrubland; Demokeya)
410 and 0.86 g C MJ^{-1} (grassland; Agoufou, Dahra, Kelma; Wankama Millet and Wankama Fallow) in the BPLUT, i.e.
411 much lower than maximum LUE measured at the Sahelian measurement sites of this study (average: 2.47 g C MJ^{-1} ;
412 range: $1.58\text{--}3.50 \text{ g C MJ}^{-1}$) (Sjöström et al., 2013; Tagesson et al., 2015a), a global estimate of $\sim 1.5 \text{ g C MJ}^{-1}$
413 (Garbulsky et al., 2010), and a savanna site in Australia (1.26 g C MJ^{-1}) (Kanniah et al., 2009).

414 Several dynamic global vegetation models have been used for decades to quantify GPP at different spatial and
415 temporal scales (Dickinson, 1983; Sellers et al., 1997). These models are generally based on the photosynthesis model
416 by Farquhar et al. (1980), a model particularly sensitive to uncertainty in photosynthetic capacity (Zhang et al., 2014).
417 This and several previous studies have shown that both photosynthetic capacity and efficiency (both α and LUE) can
418 vary considerably between seasons as well as spatially, and both within and between vegetation types (Eamus et al.,
419 2013; Garbulsky et al., 2010; Ma et al., 2014; Tagesson et al., 2015a). This variability is difficult to estimate using
420 broad values based on land cover classes, yet most models apply a constant value which can cause substantial
421 inaccuracies in the estimates of seasonal and spatial variability in GPP. This is particularly a problem in savannas that
422 ~~consists of~~ ^{comprises} several plant functional types (C3 and C4 species, and a large variability in tree/herbaceous vegetation
423 fractions) (Scholes and Archer, 1997). This study indicates the strong applicability of EO as a tool for parameterising
424 spatially explicit estimates of plant physiological variables, which could improve our ability to simulate GPP. Spatially
425 explicit estimates of GPP at a high temporal and spatial resolution are essential for environmental change studies in
426 Sahel and make a major asset for the analysis of changes in GPP, its relationship to climatic change and anthropogenic
427 forcing, and estimations of ecosystem processes and biochemical and hydrological cycles.

428 **Acknowledgements** Data is available from Fluxnet (<http://fluxnet.ornl.gov>) and CarboAfrica
429 (http://www.carboafrica.net/index_en.asp). Data for the Mali and Niger sites were made available by the AMMA-
430 CATCH regional observatory (www.amma-catch.org), which is funded by the French Institut de Recherche pour le
431 Développement (IRD) and Institut National des Sciences de l'Univers (INSU). The project was funded by the Danish
432 Council for Independent Research (DFF) Sapere Aude programme. Faculty of Science, Lund University supported the
433 Dahra and Demokeya measurements with an infrastructure grant. Ardö received support from the Swedish National
434 Space Board.

437 **References**

438 Abdi, A., Seaquist, J., Tenenbaum, D., Eklundh, L., and Ardö, J.: The supply and demand of net
439 primary production in the Sahel, *Environ. Res. Lett.*, 9, 094003, doi:10.1088/1748-9326/9/9/094003,
440 2014.

441 Ahlström, A., Raupach, M. R., Schurgers, G., Smith, B., Arneth, A., Jung, M., Reichstein, M.,
442 Canadell, J. G., Friedlingstein, P., Jain, A. K., Kato, E., Poulter, B., Sitch, S., Stocker, B. D., Viovy,
443 N., Wang, Y. P., Wiltshire, A., Zaehle, S., and Zeng, N.: The dominant role of semi-arid ecosystems